

# ADIABATIC NON-RESONANT ACCELERATION IN MAGNETIC TURBULENCE AND HARD SPECTRA OF GAMMA-RAY BURSTS

SIYAO XU<sup>1</sup> AND BING ZHANG<sup>1,2,3</sup>

*Draft version November 5, 2018*

## ABSTRACT

We introduce a non-resonant acceleration mechanism arising from the second adiabatic invariant in magnetic turbulence and apply it to study the prompt emission spectra of gamma-ray bursts (GRBs). The mechanism contains both the first- and second-order Fermi acceleration, originating from the interacting turbulent reconnection and dynamo processes. It leads to a hard electron energy distribution up to a cutoff energy at the balance between the acceleration and synchrotron cooling. The sufficient acceleration rate ensures a rapid hardening of any initial energy distribution to a power-law distribution with the index  $p \sim 1$ , which naturally produces a low-energy photon index  $\alpha \sim -1$  via the synchrotron radiation. For typical GRB parameters, the synchrotron emission can extend to a characteristic photon energy on the order of  $\sim 100$  keV.

*Subject headings:* acceleration of particles - gamma-ray burst: general-turbulence

## 1. INTRODUCTION

The gamma-ray burst (GRB) prompt emission is closely related to the physics of particle acceleration and radiation. The origin of its spectral behavior, despite the empirical description (Band et al. 1993), has not been well understood. The observed low-energy photon index has a typical value  $\alpha \sim -1$  (Preece et al. 2000; Kaneko et al. 2006; Zhang et al. 2011; Nava et al. 2011), which is difficult to reconcile with the standard model invoking the first-order Fermi acceleration and fast synchrotron cooling (Preece et al. 2002; Ghisellini et al. 2000; Kumar & Zhang 2015). Many attempts have been made to seek the solution to the problem (e.g., Brainerd 1994; Liang 1997; Mészáros & Rees 2000; Pe'er & Zhang 2006; Asano & Terasawa 2009; Asano & Mészáros 2011; Daigne et al. 2011; Uhm & Zhang 2014).

In either a Poynting-flux-dominated or a baryonic relativistic outflow, turbulence is inevitably present and participates in the electron acceleration process. The stochastic acceleration through resonant scattering with magnetic fluctuations has been used to explain the hard electron spectrum (e.g. Bykov & Mészáros 1996; Asano & Terasawa 2009; Asano & Mészáros 2011; Murase et al. 2012). Advances in turbulence theories (Goldreich & Sridhar 1995; Lazarian & Vishniac 1999) provide new insight into the problem. Turbulent reconnection, which was put forward by Lazarian & Vishniac (1999) and numerically confirmed in both non-relativistic (Kowal et al. 2009, 2012b) and relativistic (Takamoto et al. 2015) plasmas, provides an efficient dissipation mechanism of the magnetic energy in the GRB outflow. Zhang & Yan (2011) invoked a moderately Poynting-flux-dominated GRB jet and collision-induced magnetic dissipation to interpret GRB prompt emission. This ICMART model envisages significant turbulent reconnection and reconnection-driven turbulence in the emission region of GRBs. Relativistic MHD simulations (Deng et al. 2015) and Monte Carlo simulations (Zhang & Zhang 2014) confirmed

some features (e.g. efficient energy dissipation, existence of mini-jets and their effects on the lightcurves) of the original model (Zhang & Yan 2011). The large emission radius invoked in the ICMART model allows a modification of the fast synchrotron cooling theory through invoking the decrease of the magnetic field in the emission region as the jet expands in space, which can reproduce the desired  $\alpha \sim -1$  even for first-order-Fermi-accelerated electrons (probably through reconnection) (Uhm & Zhang 2014).

In magnetohydrodynamic (MHD) turbulence, the turbulent reconnection efficiently relaxes tangled field lines and facilitates turbulent motions. Meanwhile, turbulent shearing motions stretch field lines and generate magnetic fluctuations via the turbulent dynamo (Xu & Lazarian 2016). Their nonlinear interactions regulate the dynamics of MHD turbulence and affect the acceleration of the electrons for which the second adiabatic invariant applies (Brunetti & Lazarian 2016). The adiabatic condition is easily satisfied in a strongly magnetized GRB outflow, because either the gyroresonance scattering is absent with the particle Larmor radius below turbulence scales, or it is inefficient due to turbulence anisotropy (Yan & Lazarian 2002). It is the first-order Fermi process within each reconnection/dynamo region and the second-order Fermi process as particles stochastically encounter the reconnection/dynamo event. The stochastic nature originates from the balance between the annihilation and generation of magnetic fluxes in a trans-Alfvénic turbulence (Goldreich & Sridhar 1995) (hereafter GS95). In this Letter, based on the modern understanding of the dynamical nature of MHD turbulence, we analytically solve the evolution of the electron energy distribution resulting from the above adiabatic acceleration in trans-Alfvénic turbulence (§2), and demonstrate that the resultant hard energy distribution entails a hard synchrotron spectrum at low energies in the prompt GRB phase, consistent with observations (§3). A discussion of the results is in §4.

## 2. ADIABATIC ACCELERATION OF ELECTRONS IN MHD TURBULENCE

### 2.1. Energy spectrum of electrons

We consider a turbulence regime with the magnetic and kinetic energies in equipartition. It is the trans-Alfvénic

<sup>1</sup> Department of Astronomy, School of Physics, Peking University, Beijing 100871, China; syxu@pku.edu.cn

<sup>2</sup> Kavli Institute for Astronomy and Astrophysics, Peking University, Beijing 100871, China

<sup>3</sup> Department of Physics and Astronomy, University of Nevada Las Vegas, NV 89154, USA; zhang@physics.unlv.edu

turbulence described by GS95, and has been numerically tested in both non-relativistic/low- $\sigma$  (Maron & Goldreich 2001; Cho et al. 2002) and relativistic/high- $\sigma$  (Cho 2005, 2014) cases. In trans-Alfvénic turbulence, there co-exist the magnetic field line-stretching process, i.e., turbulent dynamo (Cho et al. 2009; Xu & Lazarian 2016), driven by turbulent velocities and the field line-shrinking process driven by the turbulent magnetic reconnection (Lazarian & Vishniac 1999). These two opposing processes take place at the same rate over all the turbulent scales, with the overall magnetic flux conserved.

The electrons, when they are not subject to scattering by magnetic fluctuations, undergo the first-order Fermi acceleration in reconnection regions (de Gouveia dal Pino & Lazarian 2005; Lazarian & Opher 2009) and deceleration in dynamo regions as a consequence of the second adiabatic invariant, leading to a globally diffusive energy gain. It is similar to the process that moving particles are stochastically trapped between approaching “mirrors” and receding “mirrors” (Fluegge 1961).

The energy gain/loss within each turbulent eddy follows the first-order Fermi process. Despite the large energy change, we consider the Fokker-Planck equation as a valid description, since it yields the basically identical particle spectrum as that from the statistical approach independent of the energy increment (Schneider 1993).

The evolution equation of the energy distribution function is

$$\frac{\partial N}{\partial t} = a_2 \frac{\partial}{\partial E} \left( E \frac{\partial(EN)}{\partial E} \right) - (a_{1,\text{rec}} - a_{1,\text{dyn}}) \frac{\partial(EN)}{\partial E} + \beta \frac{\partial(E^2 N)}{\partial E}, \quad (1)$$

where  $N(E, t)dE$  is the number of electrons within the energy interval from  $E$  to  $E + dE$ . The terms on the RHS represent the second- and first-order Fermi processes, and synchrotron loss, while the adiabatic expansion of the plasma and electron escape are neglected.

We consider that the turbulent eddies at the injection scale  $l_{\text{tur}}$  of the GS95 turbulence, i.e. the typical energy-containing scale, dominate the reconnection/dynamo. Provided  $r_L < l_{\text{tur}}$ , where  $r_L$  is the Larmor radius, the stochastic acceleration rate  $a_2$ , related to the comparable reconnection acceleration rate  $a_{1,\text{rec}}$  and the dynamo deceleration rate  $a_{1,\text{dyn}}$ , is independent of particle energy. It is associated with the eddy turnover rate,

$$a_2 \sim a_{1,\text{rec}} \sim a_{1,\text{dyn}} \sim \xi \frac{u_{\text{tur}}}{l_{\text{tur}}}, \quad (2)$$

where  $u_{\text{tur}}$  is the relativistic turbulent velocity at  $l_{\text{tur}}$ , and  $\xi = \Delta E/E \sim \gamma_{\text{tur}}^2$  for highly relativistic turbulence and particles to account for the energy conversion efficiency, with the turbulence Lorentz factor  $\gamma_{\text{tur}}$  (Fluegge 1961).

Therefore, Eq. (1) can be reduced to

$$\frac{\partial N}{\partial t} = a_2 \frac{\partial}{\partial E} \left( E \frac{\partial(EN)}{\partial E} \right) + \beta \frac{\partial(E^2 N)}{\partial E}. \quad (3)$$

After the substitution of the relations,  $f = EN = \exp(-\epsilon E)u(x, \tau)$ ,  $\epsilon = \beta/a_2$ ,  $x = \ln E$ ,  $\tau = a_2 t$ , and some algebra, we derive

$$\frac{\partial u}{\partial \tau} = \frac{\partial^2 u}{\partial x^2} - \frac{E}{E_{\text{cf}}} \frac{\partial u}{\partial x}, \quad (4)$$

where we define the cutoff energy corresponding to the balance between the stochastic acceleration and the synchrotron loss,

$$E_{\text{cf}} = \frac{a_2}{\beta} = \frac{3(m_e c^2)^2 a_2}{4\sigma_T c U_B}, \quad (5)$$

where  $\sigma_T$  is the Thomson cross section,  $c$  is the light speed,  $m_e$  is the electron rest mass, and  $U_B = B^2/(8\pi)$  is the magnetic energy density. Obviously in the energy range  $E \ll E_{\text{cf}}$ , Eq. (4) becomes a straightforward diffusion equation,

$$\frac{\partial u}{\partial \tau} = \frac{\partial^2 u}{\partial x^2}, \quad (6)$$

which allows us to analyze the time-dependent behavior of  $N(E, \tau)$ .

The general form of the solution to Eq. (6) is (e.g., Evans 1998),

$$u(x, \tau) = \frac{1}{2\sqrt{\pi\tau}} \int_{y_l}^{y_u} \exp\left[-\frac{(x-y)^2}{4\tau}\right] u(y, 0) dy, \quad (7)$$

with the initial functional form  $u(y, 0)$  within the range  $[y_l, y_u]$ . The Gaussian function shows that the energy distribution spreads out in energy space following  $E \sim \exp(\pm 2\sqrt{\tau})$  (Melrose 1969). Within a finite range of  $E$  with lower and upper limits  $E_l (= \exp(y_l))$  and  $E_u (= \exp(y_u))$ , there is

$$E_u = E_l \exp(2\sqrt{\tau_{lu}}), \quad \tau_{lu} = \frac{(\ln E_u - \ln E_l)^2}{4}. \quad (8)$$

After the time  $\tau_{lu}$ , the initial spectral form is essentially smeared out within the range, the behavior of  $u$  is independent of  $x$ , and thus the energy spectrum of electrons

$$N(E, \tau) = E^{-1} u(\tau) \exp\left(-\frac{E}{E_{\text{cf}}}\right) \quad (9)$$

has a universal form of  $E^{-1}$  at  $E < E_{\text{cf}}$ . The synchrotron cooling has a negligible effect on the energy distribution in the lower energy range away from  $E_{\text{cf}}$ .

## 2.2. Examples for different initial energy distributions

### (1) Delta function

Starting from an initial point source of energy with  $u(y, 0) = \delta(y - x_0)$ ,  $y \in (-\infty, +\infty)$ ,  $x_0 = \ln E_0$ ,  $u(x, \tau)$  evolves as

$$u(x, \tau) = \frac{1}{2\sqrt{\pi\tau}} \exp\left[-\frac{(x-x_0)^2}{4\tau}\right], \quad (10)$$

and thus

$$N(E, \tau) = E^{-1} \frac{1}{2\sqrt{\pi\tau}} \exp\left[-\frac{(\ln E - \ln E_0)^2}{4\tau}\right] \exp\left(-\frac{E}{E_{\text{cf}}}\right). \quad (11)$$

The Gaussian component has a negligible contribution to the spectral form at a sufficiently large  $\tau$ .

### (2) Power-law function

Given an initially steeper spectrum with the power-law index  $p_0 > 1$ ,

$$N(E, 0) = CE^{-p_0} \exp\left(-\frac{E}{E_{\text{cf}}}\right), \quad E \in (E_l, E_u), \quad (12)$$

that is,  $u(y, 0) = C \exp[(1 - p_0)y]$ , where  $C$  is an arbitrary constant, we can obtain the evolving spectrum by using Eq.

(7),

$$N(E, \tau) = E^{-1} \frac{C}{2\sqrt{\pi\tau}} \exp\left(-\frac{E}{E_{\text{cf}}}\right) \int_{y_l}^{y_u} \exp\left[-\frac{(\ln E - y)^2}{4\tau}\right] \exp[(1-p_0)y] dy, \quad (13)$$

Its asymptotic form at a short time ( $\tau \ll 1$ ) is

$$N(E, \tau) = E^{-p_0} \frac{C}{2\sqrt{\pi\tau}} \exp\left(-\frac{E}{E_{\text{cf}}}\right), \quad (14)$$

which is governed by the initial power-law shape at  $E < E_{\text{cf}}$ . Its long-time ( $\tau \sim \tau_{lu}$ ) asymptotic expression is

$$N(E, \tau) = E^{-1} \frac{C(E_u^{1-p_0} - E_l^{1-p_0})}{2(1-p_0)\sqrt{\pi\tau}} \exp\left(-\frac{E}{E_{\text{cf}}}\right), \quad (15)$$

which again recovers the universal  $E^{-1}$  power-law distribution at  $E < E_{\text{cf}}$ .

In Fig. 1, we display the electron energy distributions obtained from the numerical solution to Eq. (4). As illustrative examples, we adopt a delta function at  $E_0/E_{\text{cf}} = 2.4 \times 10^{-3}$  in Fig. 1(a), a power-law function with  $C = 1$  and  $p_0 = 2$  over the entire energy range presented in Fig. 1(b), and set  $\epsilon = 1$ . Fig. 1(c) and 1(d) show the asymptotic analytical solutions in the low-energy limit at a specified  $\tau$ , which agree well with the numerical results. As expected, irrespective of the initial spectral form, the distribution broadens and shifts in energy space and eventually conforms to the universal power-law shape  $E^{-1}$  at  $E < E_{\text{cf}}$  over the timescale of  $\tau_{lu} \approx 20$  (Eq. (8)).

To examine the effect of synchrotron cooling on the energy distribution, in Fig. 2 we present the results with an initial delta function and different  $\epsilon$  values at  $\tau = 10$ . Notice that unlike in Fig. 1 where  $E$  is normalized by  $E_{\text{cf}}$ , here we use the normalization  $E/E_0$  to show the change of the cutoff energy with varying  $\epsilon$ . As  $\epsilon$  increases, the spectral cutoff moves to a lower energy, but the distribution below the cutoff energy is unaffected and remains the  $E^{-1}$  form.

### 3. SYNCHROTRON EMISSION OF THE ACCELERATED ELECTRONS

The above adiabatic acceleration of electrons arising in trans-Alfvénic turbulence leads to a hard electron energy distribution (see Eq. (9)), corresponding to

$$N(\gamma_e) \sim \gamma_e^{-p} \exp\left(-\frac{\gamma_e}{\gamma_{e,\text{cf}}}\right), \quad p = 1, \quad (16)$$

where  $p$  is the power-law index,  $\gamma_e$  is the electron Lorentz factor, and  $\gamma_{e,\text{cf}} = E_{\text{cf}}/m_e c^2$ .

According to the relation between  $p$  and the index  $\alpha$  of the synchrotron photon number spectrum (Rybicki & Lightman 1979), there is

$$N(\nu) \sim \nu^\alpha \exp\left(-\left(\frac{\nu}{\nu_c}\right)^{\frac{1}{2}}\right), \quad \alpha = -\frac{p+1}{2} = -1, \quad (17)$$

where the  $\delta$ -function approximation for the single-electron spectrum is made. This is the typical low-energy photon spectral index of GRBs (Preece et al. 2000; Kaneko et al. 2006; Zhang et al. 2011; Nava et al. 2011).

Unlike a soft distribution with  $p > 2$ , for which the lower cutoff energy accounts for the characteristic electron energy

and synchrotron frequency (e.g. Zhang & Mészáros 2004; Piran 2004), as regards a hard distribution, the upper cutoff energy  $E_{\text{cf}}$  is more significant as it dominates the electron energy density, and may characterize the peak energy of the  $\nu F_\nu \propto \nu^2 N(\nu)$  spectrum (Dai & Cheng 2001).  $E_{\text{cf}}$  depends on the acceleration mechanism (Eq. (2), (5)),

$$E_{\text{cf}} = \frac{\xi u_{\text{tur}}}{l_{\text{tur}} \beta} = \frac{6\pi\xi(m_e c^2)^2}{\sigma_T B^2 l_{\text{tur}}}, \quad (18)$$

where  $u_{\text{tur}}$  is approximately equal to  $c$  for relativistic turbulence.

In the case of reconnection-driven turbulence, the thickness of the turbulent region increases with time, as indicated by the numerical results in Kowal et al. (2017). Meanwhile, the magnetic field strength  $B$  decays with time (Pe'er & Zhang 2006; Uhm & Zhang 2014; Zhao et al. 2014). The comoving-frame  $B$  during the GRB prompt phase is estimated as (e.g. Zhang & Mészáros 2002)

$$B = \sqrt{\frac{2}{c}} L^{\frac{1}{2}} r^{-1} \Gamma^{-1}, \quad (19)$$

where  $L$  is the total outflow luminosity of the GRB,  $r$  is the distance of the emission region from the central engine, and  $\Gamma$  is the Lorentz factor of the outflow. We assume the following relation between  $l_{\text{tur}}$  and  $B$  to account for their anticorrelation,

$$l_{\text{tur}} = l_0 \left(\frac{B}{B_0}\right)^{-\zeta}, \quad \zeta > 0, \quad (20)$$

where  $l_0$  and  $B_0$  are normalization parameters. Then  $E_{\text{cf}}$  in Eq. (18) can be expressed as

$$E_{\text{cf}} = \frac{6\pi\xi(m_e c^2)^2}{\sigma_T B_0^\zeta l_0} B^{\zeta-2}. \quad (21)$$

The corresponding electron Lorentz factor is

$$\gamma_{e,\text{cf}} = \frac{6\pi\xi m_e c^2}{\sigma_T B_0^\zeta l_0} B^{\zeta-2}, \quad (22)$$

and the emitted photon energy in the observer frame is

$$\begin{aligned} E_{s,\text{obs}} &= (h\nu_{\text{cf}})_{\text{obs}} \\ &= \hbar \frac{eB}{m_e c} \gamma_{e,\text{cf}}^2 \Gamma(1+z)^{-1} \\ &= \hbar m_e c^3 e \left(\frac{6\pi\xi}{\sigma_T B_0^\zeta l_0}\right)^2 \Gamma(1+z)^{-1} B^{2\zeta-3}, \end{aligned} \quad (23)$$

where  $h$  is the Planck constant,  $e$  is the electron charge, and  $z$  is the redshift. Inserting Eq. (19), the above equation becomes

$$\begin{aligned} E_{s,\text{obs}} &= 2^{\zeta-\frac{3}{2}} \hbar m_e c^{-\zeta+\frac{3}{2}} e \left(\frac{6\pi\xi}{\sigma_T B_0^\zeta l_0}\right)^2 \\ &\quad \Gamma^{-2\zeta+4} (1+z)^{-1} L^{\zeta-\frac{3}{2}} r^{-2\zeta+3}. \end{aligned} \quad (24)$$

The dependence of  $E_{s,\text{obs}}$  on  $\Gamma$ ,  $L$ , and  $r$  is determined by the exact value of  $\zeta$ . Based on the empirical tight correlation among the peak energy,  $\Gamma$ , and  $L$  suggested by observations (Liang et al. 2015), we adopt  $\zeta \simeq 2.1$ . By together assuming  $\xi = 10^4$ ,  $B_0 = 10^5 \text{G}$ ,  $l_0 = 2 \times 10^9 \text{cm}$ , and using other typical parameters  $\Gamma = 100\Gamma_2$ ,  $L = 10^{52} \text{erg s}^{-1} L_{52}$ ,  $r =$

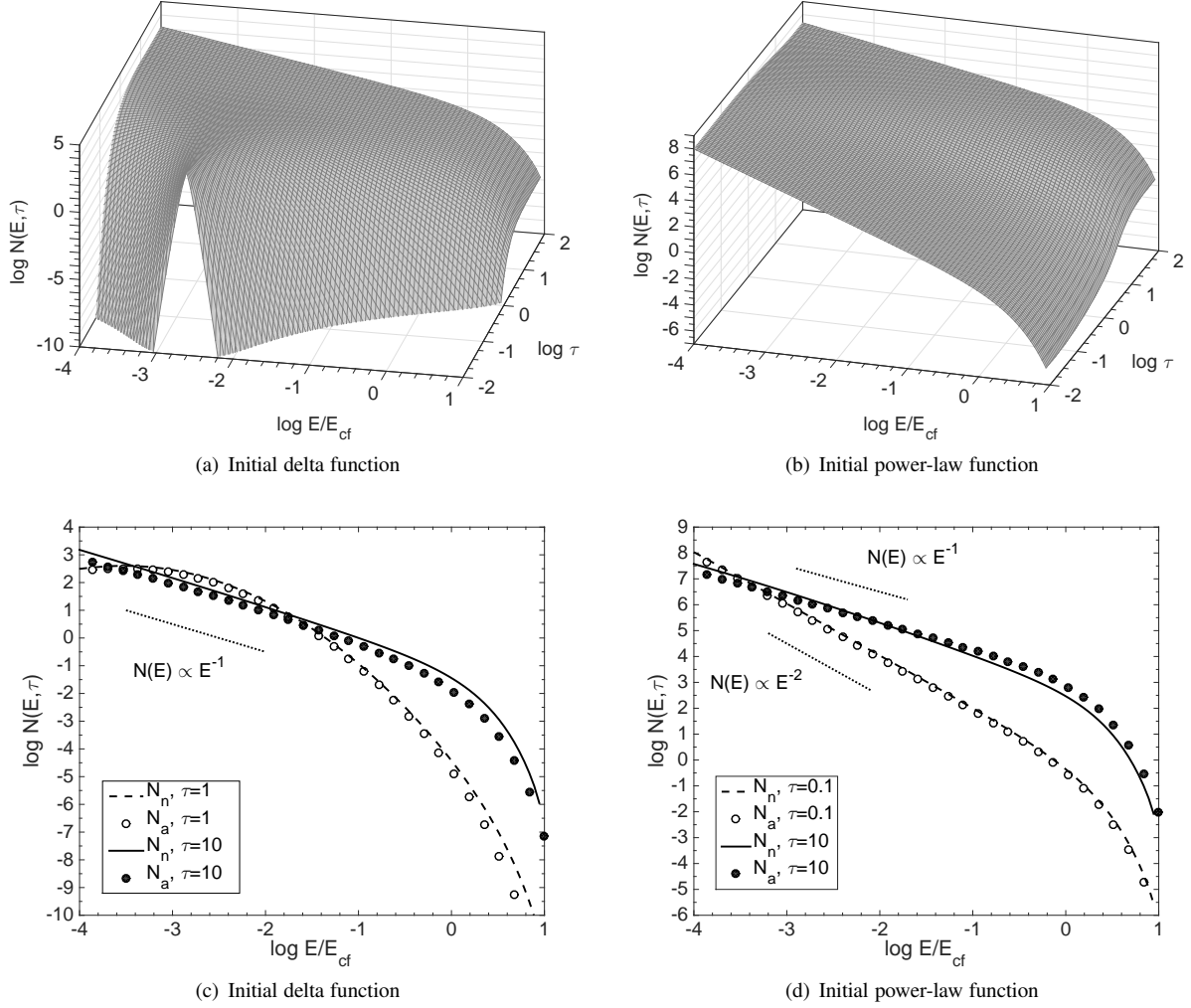


FIG. 1.— (a), (b) Temporal evolution of the energy distribution of electrons from the numerical solution to Eq. (4). (c), (d) The spectral distribution at a specified  $\tau$ . “ $N_n$ ” and “ $N_a$ ” denote the numerical and analytical results, respectively. The analytical results in (c) are from Eq. (11), and in (d) are from Eq. (14) for  $\tau = 0.1$  and Eq. (15) for  $\tau = 10$ .

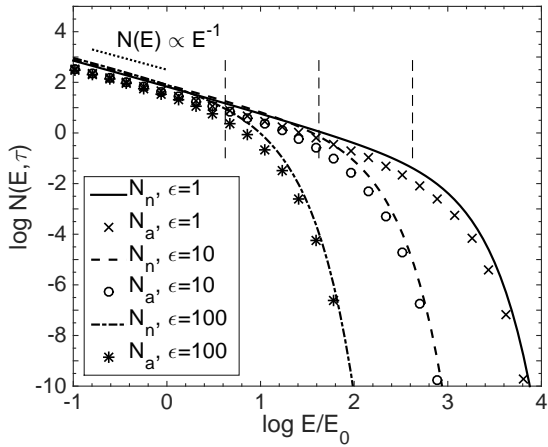


FIG. 2.— The energy distribution with different  $\epsilon$  values at  $\tau = 10$ . The vertical dashed lines indicate the positions of  $E_{cf}$ .

$10^{15} \text{cm} r_{15}$ , Eq. (24) gives

$$E_{s,\text{obs}} \simeq 385 \text{keV} \left( \frac{1+z}{2} \right)^{-1} \Gamma_2^{-0.2} L_{52}^{0.6} r_{15}^{-1.2}. \quad (25)$$

Besides, we can also estimate the timescale for an initial energy distribution with the index  $p_0$  to evolve to a hard spectrum (Eq. (2), (8), (19), (20)),

$$\begin{aligned} t_{lu} &= \frac{\tau_{lu}}{a_2} = \frac{1}{4\xi} \left[ \ln \left( \frac{E_u}{E_l} \right) \right]^2 \frac{l_0}{u_{\text{tur}}} \left( \frac{B}{B_0} \right)^{-\zeta} \\ &= \frac{1}{4\xi} \left( \frac{2}{c} \right)^{-\zeta} \left[ \ln \left( \frac{E_u}{E_l} \right) \right]^2 \frac{B_0^\zeta l_0}{u_{\text{tur}}} \Gamma_2^\zeta L^{-\frac{\zeta}{2}} r^\zeta \quad (26) \\ &= 3 \times 10^{-2} \text{s} F(E_u, E_l)_2 \Gamma_2^{2.1} L_{52}^{-1.05} r_{15}^{2.1}, \end{aligned}$$

with  $[\ln(E_u/E_l)]^2 = 10^2 F(E_u, E_l)_2$ . Irrespective of the value of  $p_0$  (which can be larger or smaller than one), after  $t_{lu}$ , the electron distribution index  $p$  approaches one under the effect of the adiabatic acceleration.

#### 4. DISCUSSION

We have applied the adiabatic acceleration mechanism in MHD turbulence, which has been earlier identified by Brunetti & Lazarian (2016), and derived a robust electron energy distribution index  $p \sim 1$  and a synchrotron low-energy photon index  $\alpha \sim -1$ , generally consistent with the observations. The estimated characteristic synchrotron emission energy with proper turbulence parameters required is in the sub-MeV regime, which is also consistent with the observations. A hard particle spectrum due to stochastic accelerations was also discussed within the GRB context by, e.g. Bykov & Mészáros (1996); Asano & Terasawa (2009); Asano & Mészáros (2011); Murase et al. (2012). However, here we consider a different non-resonant acceleration related to the reconnection and dynamo processes in MHD turbulence, and strictly derive  $p = 1$  analytically.

Depending on the relation between the magnetic and turbulent kinetic energies, turbulence has various regimes. In the magnetic energy-dominated turbulence, the first-order Fermi acceleration during the turbulent reconnection (de Gouveia dal Pino & Lazarian 2005; Kowal et al. 2012a) can dominate the electron acceleration and shape the initial energy distribution. With the conversion of magnetic energy to turbulent kinetic energy, the acceleration process be-

comes globally stochastic in the trans-Alfvénic turbulence and rapidly flattens the electron energy distribution. To more realistically model the synchrotron spectrum, one should consider the interplay between the particle injection and acceleration, with synchrotron cooling incorporated self-consistently (S. Xu et al. 2017, in preparation).

Besides the GRB prompt emission spectrum, observations of active galactic nuclei, blazars, and pulsar wind nebulae also reveal a hard electron distribution (e.g., Shen et al. 2006; Hayashida et al. 2015). The acceleration mechanism presented here is a promising candidate for interpreting the spectral hardness in various scenarios.

We thank the anonymous referee for insightful comments. SX is grateful for the support from the Pilot-B program for gravitational wave astrophysics of the Chinese Academy of Sciences and the Research Corporation for Scientific Advancement during her visit at the Aspen Center for Physics. SX thanks Yuanpei Yuan for valuable discussions. This work is partially supported by the National Basic Research Program (973 Program) of China under grant No. 2014CB845800.

#### REFERENCES

- Asano, K., & Mészáros, P. 2011, *ApJ*, 739, 103  
 Asano, K., & Terasawa, T. 2009, *ApJ*, 705, 1714  
 Band, D., et al. 1993, *ApJ*, 413, 281  
 Bykov, A.M., & Mészáros, P. 1996, *ApJ*, 461, 37  
 Brainerd, J. J. 1994, *ApJ*, 428, 21  
 Brunetti, G., & Lazarian, A. 2016, *MNRAS*, 458, 2584  
 Cho, J. 2005, *ApJ*, 621, 324  
 —, 2014, *Journal of Korean Physical Society*, 65, 871  
 Cho, J., Lazarian, A., & Vishniac, E. T. 2002, *ApJ*, 564, 291  
 Cho, J., Vishniac, E. T., Beresnyak, A., Lazarian, A., & Ryu, D. 2009, *ApJ*, 693, 1449  
 Dai, Z. G., & Cheng, K. S. 2001, *ApJ*, 558, L109  
 Daigne, F., Bošnjak, Ž., & Dubus, G. 2011, *A&A*, 526, A110  
 de Gouveia dal Pino, E. M., & Lazarian, A. 2005, *A&A*, 441, 845  
 Deng, W., Li, H., Zhang, B., & Li, S. 2015, *ApJ*, 805, 163  
 Evans, L. 1998, *Partial Differential Equations* (American Mathematical Society)  
 Fluegge, S. 1961, in *Handbuch der Physik: Kosmische Strahlung I*, ed. Fluegge, S. (Berlin: Springer), 26  
 Ghisellini, G., Celotti, A., & Lazzati, D. 2000, *MNRAS*, 313, L1  
 Goldreich, P., & Sridhar, S. 1995, *ApJ*, 438, 763  
 Hayashida, M., et al. 2015, *ApJ*, 807, 79  
 Kaneko, Y., Preece, R. D., Briggs, M. S., Paciesas, W. S., Meegan, C. A., & Band, D. L. 2006, *ApJS*, 166, 298  
 Kowal, G., de Gouveia Dal Pino, E. M., & Lazarian, A. 2012a, *Physical Review Letters*, 108, 241102  
 Kowal, G., Falceta-Gonçalves, D. A., Lazarian, A., & Vishniac, E. T. 2017, *ApJ*, 838, 91  
 Kowal, G., Lazarian, A., Vishniac, E. T., & Otmianowska-Mazur, K. 2009, in *Revista Mexicana de Astronomía y Astrofísica Conference Series*, Vol. 36, *Revista Mexicana de Astronomía y Astrofísica Conference Series*, 89–96  
 Kowal, G., Lazarian, A., Vishniac, E. T., & Otmianowska-Mazur, K. 2012b, *Nonlinear Processes in Geophysics*, 19, 297  
 Kumar, P., & Zhang, B. 2015, *Phys. Rep.*, 561, 1  
 Lazarian, A., & Opher, M. 2009, *ApJ*, 703, 8  
 Lazarian, A., & Vishniac, E. T. 1999, *ApJ*, 517, 700  
 Liang, E. P. 1997, *ApJ*, 491, L15  
 Liang, E.-W., Lin, T.-T., Lü, J., Lu, R.-J., Zhang, J., & Zhang, B. 2015, *ApJ*, 813, 116  
 Maron, J., & Goldreich, P. 2001, *ApJ*, 554, 1175  
 Melrose, D. B. 1969, *Ap&SS*, 5, 131  
 Mészáros, P., & Rees, M. J. 2000, *ApJ*, 530, 292  
 Murase, K., Asano, K., Terasawa, T., & Mészáros, P. 2012, *ApJ*, 746, 164  
 Nava, L., Ghirlanda, G., Ghisellini, G., & Celotti, A. 2011, *A&A*, 530, A21  
 Pe’er, A., & Zhang, B. 2006, *ApJ*, 653, 454  
 Piran, T. 2004, *Reviews of Modern Physics*, 76, 1143  
 Preece, R. D., Briggs, M. S., Giblin, T. W., Mallozzi, R. S., Pendleton, G. N., Paciesas, W. S., & Band, D. L. 2002, *ApJ*, 581, 1248  
 Preece, R. D., Briggs, M. S., Mallozzi, R. S., Pendleton, G. N., Paciesas, W. S., & Band, D. L. 2000, *ApJS*, 126, 19  
 Rybicki, G. B., & Lightman, A. P. 1979, *Radiative processes in astrophysics*  
 Shen, R., Kumar, P., & Robinson, E. L. 2006, *MNRAS*, 371, 1441  
 Schneider, P. 1993, *A&A*, 269, 13  
 Takamoto, M., Inoue, T., & Lazarian, A. 2015, *ApJ*, 815, 16  
 Uhm, Z. L., & Zhang, B. 2014, *Nature Physics*, 10, 351  
 Xu, S., & Lazarian, A. 2016, *ApJ*, 833, 215  
 Zhang, B., & Mészáros, P. 2002, *ApJ*, 581, 1236  
 —, 2004, *International Journal of Modern Physics A*, 19, 2385  
 Zhang, B., & Yan, H. 2011, *ApJ*, 726, 90  
 Zhang, B., & Zhang, B. 2014, *ApJ*, 782, 92  
 Zhang, B.-B., et al. 2011, *ApJ*, 730, 141  
 Zhao, X., Li, Z., Liu, X., Zhang, B.-b., Bai, J., & Mészáros, P. 2014, *ApJ*, 780, 12  
 Yan, H., & Lazarian, A. 2002, *Phys. Rev. Lett.*, 89, 1102